DOI 10.1007/s11182-020-02032-4

Russian Physics Journal, Vol. 63, No. 2, June, 2020 (Russian Original No. 2, February, 2020)

PHYSICS OF SEMICONDUCTORS AND QUANTUM ELECTRONICS

MORPHOLOGY, STRUCTURE, AND OPTICAL PROPERTIES OF SnO (x) FILMS

A. I. Nikiforov,[1,2] V. A. Timofeev,[1] V. I. Mashanov,[1] I. A. Azarov,[1,4] I. D. Loshkarev,[1] I. V. Korol'kov,[3,4] T. A. Gavrilova,[1] and M. Yu. Esin[1]

UDC 621.315.592

The paper presents the morphological, structural, and optical properties of nanostructured SnO *(x) films obtained by molecular beam epitaxy using deposition of tin in an oxygen flux on an oxidized silicon substrate as a function of the annealing temperature of the synthesized structure. The effect of annealing temperature on the structural and phase state of the films is established. The orthorhombic phase of* SnO_2 *was observed after annealing in air at 500°C. An increase in the annealing temperature up to 800°C leads to the appearance of small fraction of the tetragonal phase of* SnO_2*. The effect of the crystal structure on the optical properties of tin oxide films is shown. Ellipsometry revealed a sharp change in the optical constants of the film near the annealing temperature of 500°C. The observed wide absorption band in the range 1.9–3.4 eV is apparently associated with small (approximately 1%) amount of unoxidized metal Sn clusters. Photoluminescence in a wide range of 450–850 nm with a maximum at ~600 nm is observed. An increase in the annealing temperature from 500 to 800°C leads to an increase in the PL intensity by almost a factor of 6.*

Keywords: tin oxide, epitaxy, nanostructures, X-ray diffraction, absorption coefficient.

INTRODUCTION

Tin oxides belong to the class of materials that combine high electrical conductivity, optical transparency in the visible range and absorption in the ultraviolet range, as well as reflection of infrared light due to the plasma reflection edge. There are a large number of transparent conductive oxides (TCO). The most known are oxides based on such metals as In, Sn, Zn, Ga, and Cd [1, 2]. The main requirements to the transparent conductive films are low resistivity (<0.001 Ω·cm), high optical transparency (>80%), and a wide band gap (>3.5 eV). To date, the most widely used is the tin doped indium oxide (In_2O_3). Indium, as the main element of oxide, is contained in the earth's crust, but its content is only 0.00001% and it is a by-product of the Zn and Pb production. Therefore, the production of tin doped In_2O_3 films requires significant financial investments. Among all the TCO, tin oxide films are affordable, have attractive electronic, optical, and electrochemical properties [3], chemical stability to acids and bases, are thermally stable and mechanically

[1]Rzhanov Institute of Semiconductor Physics of the Siberian Branch of the Russian Academy of Sciences, Novosibirsk, Russia, e-mail: nikif@isp.nsc.ru; Vyacheslav.t@isp.nsc.ru; mash@isp.nsc.ru; idl@isp.nsc.ru; gavr@isp.nsc.ru; yesinmisha@gmail.com; [2]National Research Tomsk State University, Tomsk, Russia; [3]Nikolaev Institute of Inorganic Chemistry of the Siberian Branch of the Russian Academy of Sciences, Novosibirsk, Russia, e-mail: korolkov@niic.nsc.ru; [4]Novosibirsk State University, Novosibirsk, Russia, e-mail: azarov_ivan@mail.ru; Translated from Izvestiya Vysshikh Uchebnykh Zavedenii, Fizika, No. 2, pp. 85–90, February, 2020. Original article submitted December 16, 2019.

1064-8887/20/6302-0276 ©2020 Springer Science+Business Media, LLC

strong [4]. Compared to tin oxides, the known films of zinc oxide (ZnO) are unstable to acids and alkalis. Tin oxide films have a higher concentration of charge carriers and transmission in the visible range [5].

Recently, tin oxide films have attracted great attention of scientists and technologists in connection with their possible applications in solid state gas sensors, in electrodes for electroluminescent displays, in protective coatings, in solar cells, and in the transparent field-effect transistors [6, 7]. Two main tin oxides are being studied: SnO and SnO_2. The existence of these two oxides is associated with the double valency of Sn with oxidation states of +2 and +4. Both of these oxides are known to be wide-gap semiconductors with a rutile structure (tetragonal lattice) for SnO_2 and a PbO structure for SnO [6]. Tin dioxide is a wide-gap *n*-type semiconductor, has a band gap from 3.6 to 4 eV [8, 9] and a transparency of more than 85% [10]. SnO_2 films were obtained by such methods as molecular beam epitaxy [11], pulsed laser deposition [12], electron beam evaporation [13], sputtering [14], and the sol–gel process [15]. In most works, SnO_2 films are polycrystalline. Tin monoxide is a *p*-type wide-gap semiconductor, but there is little data on its band gap. It lies in the range from 2.7 to 3.4 eV [6]. The large absorption coefficient indicates predominantly direct optical transitions in the ultraviolet region. SnO films were formed by electron beam evaporation [16], pulsed laser deposition [17], magnetron sputtering [18], and atomic layer deposition [19]. In [20, 21], in addition to structural properties, optical and electronic properties are presented. It was shown that an increase in pressure leads to the formation of nanocrystalline orthorhombic SnO and an increase in transmission in the ultraviolet, visible, and near infrared regions of the spectrum. An increase in the substrate temperature leads to the formation of a hydrophilic coating containing the phases of orthorhombic SnO and tetragonal SnO_2 and to the change in the type of conductivity to *n*-type. A shift in the absorption edge and an increase in the band gap were observed with increasing pressure or substrate temperature.

The aim of this work is to study the transformation process of the morphology and structure of SnO_2 and SnO films obtained by molecular beam epitaxy (MBE). The structural and phase states of the films will be established depending on the conditions of formation and subsequent annealing, and the effect of the crystal structure on the optical properties of tin oxide films will be shown.

RESULTS AND DISCUSSION

Samples with nanostructured SnO (x) films were obtained on the Katun-C MBE setup. The chamber is equipped with an electron beam evaporator (EBE) for silicon and an effusion cell for tin. The Sn films are deposited on a Si(111) substrate with a 100 nm thick SiO_2 layer at a Sn deposition rate of 0.28 Å/s in the presence of oxygen. The pressure during growth was 10^{-6} Torr. The temperature of the substrate was chosen below the melting temperature of Sn (approximately 180°C). A silicon EBE was used to ionize oxygen molecules. The electrons in the EBE had a high energy of about 5 keV and the electron emission current ranged from 0 to 85 mA. The obtained structures were annealed at atmospheric pressure in the temperature range of 200–1000°C. Temperature control was carried out using a chromel-alumel thermocouple, as well as a double laser infrared thermometer. The surface morphology and structure during growth in the MBE chamber were controlled by the reflection high-energy electron diffraction (RHEED). In addition, the film morphology was analyzed using a scanning electron microscope (SEM) Hitachi SU8220. The SEM system allows elemental analysis of the grown samples, since it additionally includes the EDX (Energy Dispersive X-ray Spectroscopy) technique with a Bruker detector. The XFlash 5060F QUAD detector, which is part of the SEM equipment, was used to analyze the radiation energy of the X-ray spectrum. The crystal structure and phase analysis were performed by X-ray diffraction (XRD) method using a powder X-ray diffraction system (Shimadzu XRD-7000, CuK_α radiation, $\lambda = 1.5416$ Å, and OneSight linear detector) in the range of 2θ from 10 to 65°. Diffraction patterns were analyzed by powder diffractometry (PDF) (Powder Diffraction File database, 2010 edition of the International Center for Diffraction Data, Pennsylvania, USA). Optical constants in the wavelength range of 250–1000 nm were studied by ellipsometry using instruments developed and manufactured at the Institute of Semiconductor Physics SB RAS [22]. The film was considered uniform in depth. Therefore, the reconstructed dielectric functions and thickness are effective. To excite photoluminescence (PL), a HeCd laser with a wavelength of 325 nm and an excitation power of 2 mW was used. The PL was recorded by a spectrometer equipped with both a nitrogen-cooled silicon CCD matrix and a cooled photoelectronic multiplier with an S-20 type photocathode. The measurements were carried out at room temperature.

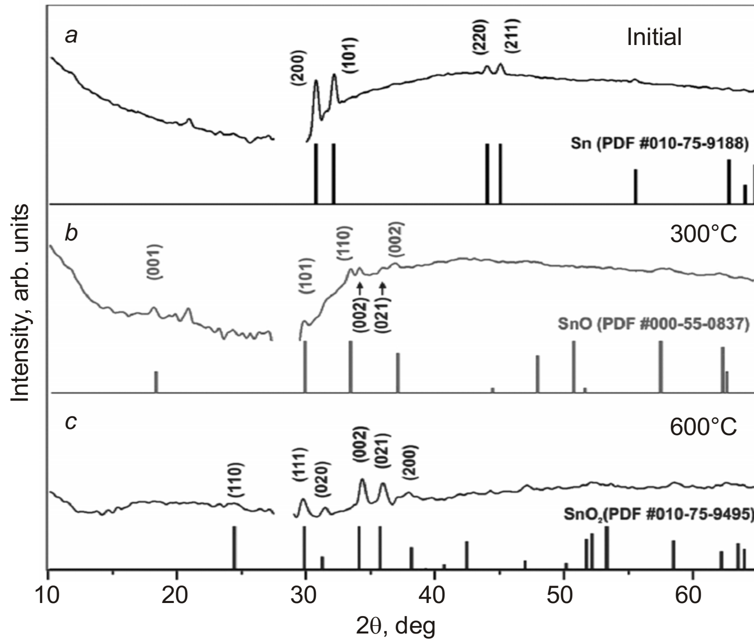

Fig. 1. Experimental diffraction reflection curves and bar charts from the PDF database for the initial sample (*a*) and for samples annealed at 300°C (*b*) and 500°C (*c*).

The RHEED control of the tin film deposition process showed that the film is polycrystalline. Such a conclusion is indicated by the presence of characteristic rings in the diffraction pattern. Next, the samples were annealed at atmospheric pressure. To determine the crystal structure and phase composition, X-ray powder diffraction (XRD) was used. The angle range 2θ = 28–29° in the diffraction measurements was excluded, since it contains an intense peak from the Si(111) substrate. Diffraction curves (X-ray diffraction patterns) for the initial sample, as well as for samples annealed at 300 and 600°C, and the tabular (calculated) diffraction patterns for the Sn, SnO, and SnO_2 phases are shown in Fig. 1. The annealing of all films lasted 1 h. The diffraction peaks of the initial sample at 2θ = 30.6, 32.0, 43.9, and 44.9° correspond to (200), (101), (220), and (211) planes of the tetragonal Sn crystal (β-Sn, PDF # 010-75-9188). According to the RHEED data, the Sn film is polycrystalline. An increase in the annealing temperature leads to the appearance of the SnO phase. The sample annealed at 300°C contains mainly a SnO phase (Romarchite Tin Oxide, PDF # 000-55-0837) with a tetragonal structure. In addition to the SnO phase, the peaks (002) and (021) are observed, which are due to the appearance of SnO_2 at this temperature. The transformation of the film crystalline structure into tin oxide (SnO_2) occurs at 500°C. The diffraction peaks at 2θ = 29.9, 31.3, 34.2, 35.8, and 38.2° correspond to the planes (111), (020), (002), (021), and (200) of orthorhombic SnO_2 crystals (o-SnO_2, PDF # 010-75-9495) and are shown in Fig. 1*c* for the sample annealed at 600°C. A similar result with orthorhombic SnO_2 was obtained for tin oxide nanowires [23]. The data of X-ray phase analysis indicate a transition from a tetragonal SnO to an orthorhombic SnO_2, which is single-phase. The orthorhombic phase of SnO_2 was observed at annealing temperatures above 500°C. A further increase in temperature to 800°C did not change the SnO_2 phase. Nevertheless, in addition to the orthorhombic SnO_2, a small tetragonal part of SnO_2 was found.

To determine the surface morphology and structure of the grown films, atomic force microscopy (AFM) and SEM studies were performed. It was established that SnO (*x*) films are nanostructured. The SEM images of the SnO (*x*) film surface after annealing at temperatures of 400 and 800°C are shown in Figs. 2*a*, *c*. Figures 2*b* and 2*d* show the histograms of the amount distribution over the base size, which indicate the formation of a bimodal island distribution at low annealing temperature (Fig. 2*b*). The density of islands and their average size reach $7.2 \cdot 10^9$ cm^{-2} and 87.5 nm, respectively. It is important to note that in the region of 70 and 100 nm, two maxima are observed. An increase in the SnO (*x*) film annealing temperature to 800°C leads to the formation of a more uniform size distribution of islands. The

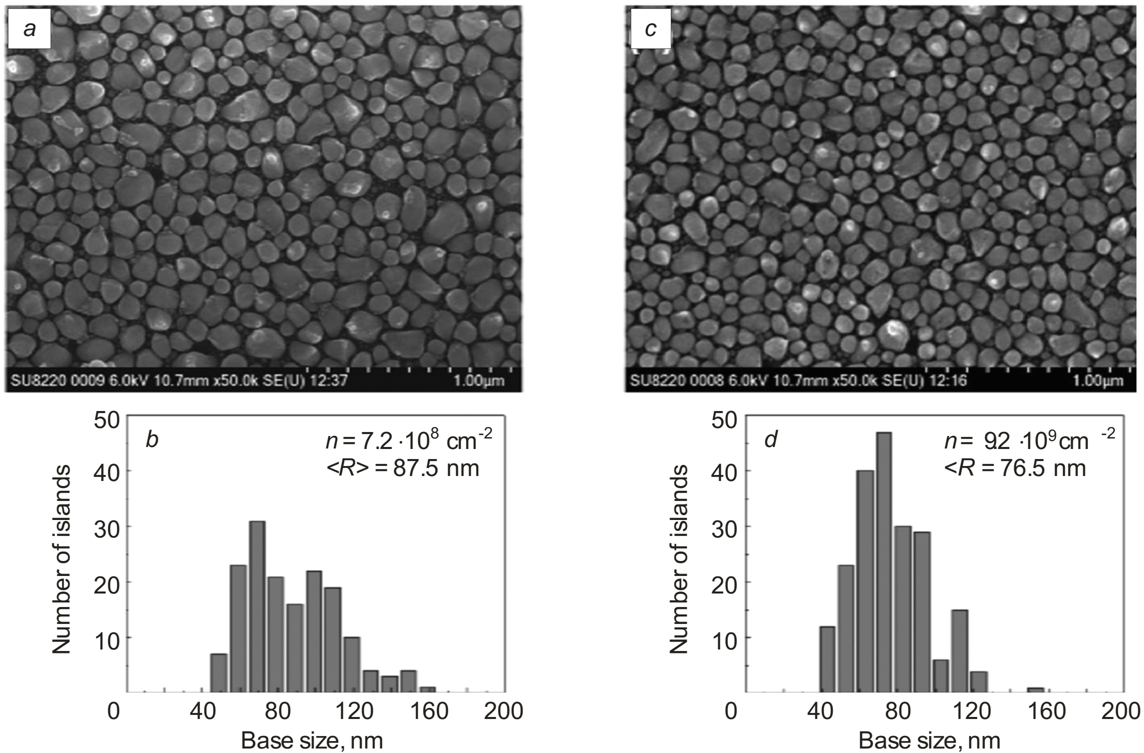

Fig. 2. SEM image of the surface of SnO (*x*) films and the corresponding size distribution after annealing at: 400°C (*a*, *b*) and 800°C (*c*, *d*).

ratio of the maxima corresponding to 70 and 110 nm, shown in Fig. 2*d*, increases with respect to the value obtained at 400°C (Fig. 2*b*). At an annealing temperature of 800°C, the average size of islands is 76.5 nm. An analysis of the surface morphology of the films was additionally carried out by the AFM method. The AFM data on the surface morphology of the obtained films are in good agreement with the SEM data. The islands contained in the nanostructured SnO (*x*) film begin to decompose into the smaller nanoclusters during annealing at 1000°C. However, the original islands still retain their boundaries. Changes in the morphology observed during film annealing can affect both optical constants and optical properties of the obtained SnO (*x*) films. Elemental analysis of the grown samples was performed by EDX spectroscopy. Based on the map of elements, it can be concluded that the islands are enriched with Sn and O. Therefore, the X-ray diffractometry signal is formed from these elements.

Optical constants of nanostructured SnO (*x*) films were studied by ellipsometry under various growth and annealing conditions. The dependence of the absorption coefficient for the SnO (*x*) film on the temperature of atmospheric annealing is shown in Fig. 3.

High absorption coefficients correspond to a high content of metallic Sn. The absorption edge shifts from 3.76 eV at 550°C to 3.9 eV at temperatures of 700°C and higher. In addition, absorption occurs in the visible range of the spectrum. It is inherited from the initial film and may indicate a low concentration of unoxidized metal Sn clusters. This concentration is approximately 1%. The film thickness varies nonmonotonously during the annealing process. First, it grows from 45 to 65 nm, since active oxidation continues up to 500°C. Then, at temperatures higher than 600°C, the film thickness begins to decrease. Annealing of the film at temperatures of 900–1000°C leads to its compaction. Optical constants track the phase and morphological changes in the film. It is important to note a sharp change in the behavior of optical constants near the temperature of 500°C. Apparently, this temperature is characteristic of the oxidation process. The pronounced absorption edge observed in the short-wavelength region at higher temperatures disappears at temperatures below 500°C. Energies of 3.7–3.9 eV correspond to the band gap of SnO_2 [24].

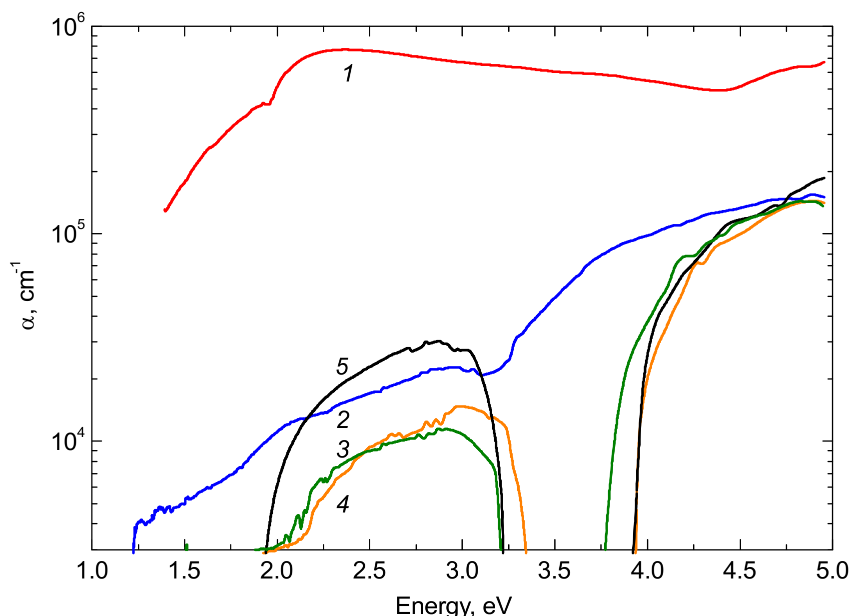

Fig. 3. Dependence of absorption coefficient for the SnO (*x*) film on the annealing temperature at atmospheric conditions: initial (*1*), 500°C (*2*), 550°C (*3*), 800°C (*4*), and 1000°C (*5*).

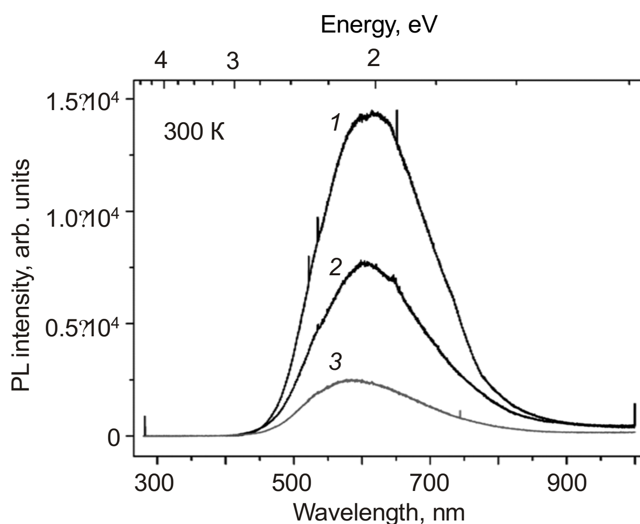

Fig. 4. PL intensity spectra obtained at room temperature and an excitation wavelength of 325 nm: 800°C (*1*), 700°C (*2*), and 500°C (*3*).

According to our estimates, the film porosity can reach 40%. This indicates the island character of the film, which is confirmed by the results of scanning electron microscopy and atomic force microscopy.

Optical properties of the films were studied by photoluminescence (PL). Figure 4 shows the PL spectra obtained for the SnO (*x*) film. The numbers indicate the spectra corresponding to some film annealing temperatures. A wide PL region is observed in the range 450–850 nm with a PL maximum at ~ 600 nm. Usually, PL in this range is associated with the crystal defects or defect levels that appear during film growth or annealing. An increase in the annealing temperature from 500 to 800°C leads to an almost 6-fold increase in intensity. As shown in Fig. 4, absorption

in the visible range is associated with a small concentration of tin crystallites. Therefore, an increase in PL with increasing annealing temperature can occur as a result of further oxidation of the film and the formation of tin islands several nanometers in size, which contribute to the radiative recombination.

CONCLUSIONS

Nanostructured SnO (*x*) films with a polycrystalline structure were obtained by molecular beam epitaxy using deposition of tin in an oxygen flux on an oxidized silicon substrate. It is found that their structural state depends on the temperature of the subsequent annealing in atmospheric conditions. It is shown that at annealing temperatures higher than 500°C, the phase state of the films changes with the transformation of their crystal structure from a tetragonal SnO to an orthorhombic SnO_2. Their optical properties, especially the absorption coefficient, change, and it was found that the absorption edge shifts from 3.76 eV at 550°C to 3.9 eV at temperatures of 700°C and above. In the obtained films, a wide PL region is observed in the range of 450–850 nm with a PL maximum at ~ 600 nm. Photoluminescence may be associated with the formation of nanosized Sn islands during the SnO (*x*) film oxidation, which contribute to the radiative recombination.

This work was supported in part by the RFBR grants Nos. 18-32-20064, 18-42-540018, and 18-52-41006.

REFERENCES

1. K. L. Chopra, S. Major, and D. K. Pandya, Thin Solid Films, **102**, 1–46 (1983).
2. T. J. Coutts, D. L. Young, and X. Li, MRS Bull., **25**, 58–65 (2000).
3. J. Sun, A. Lu, L. Wang, *et al*., Nanotechnology, **20**, 335204 (2009).
4. E. Elangovan, M. P. Singh, M. S. Dharmaprakash, and K. Ramamurthi, J. Optoelectron. Adv. Mater., **6**, 197–203 (2004).
5. H. S. So, J.-W. Park, D. H. Jung, *et al*., J. Appl. Phys., **118**, 085303 (2015).
6. M. Batzill and U. Diebold, Prog. Surf. Sci., **79**, No. 47, 154 (2005).
7. R. E. Presley, C. L. Munsee, C.-H. Park, *et al*., J. Phys. D, **37**, 2810–2813 (2004).
8. D. P. Joseph, P. Renugambal, M. Saravanan, *et al*., Thin Solid Films, **517**, 6129–6136 (2009).
9. Q.-H. Wu, J. Song, J. Kang, *et al*., Mater. Lett., **61**, 3679–3684 (2007).
10. Y. Kim, J. H. Jang, J. S. Kim, *et al*., Mater. Sci. Eng. B, **177**, 1470–1475 (2012).
11. M. Batzill, J. M. Burst, and U. Diebold, Thin Solid Films, **484**, 132–139 (2012).
12. H. Kim and A. Piqué, Appl. Phys. Lett., **84**, 218–220 (2004).
13. E. Kh. Shokr, M. M. Wakkad, H. A. Abd El-Ghanny, and H. M. Ali, J. Phys. Chem. Solids, **61**, 75–85 (2000).
14. J. Ma, Y. Wang, F. Ji, *et al*., Mater. Lett., **59**, 2142–2145 (2005).
15. J. C. Li and H. L. Yuan, Cryst. Res. Technol., **52**, 1700183 (2017).
16. R. Sethi, S. Ahmad, A. Aziz, and A. M. Siddiqui, Adv. Mater. Radiat. Physics (AMRP-2015), **1675**, 030039 (2015).
17. L. Y. Liang, Z. M. Liu, H. T. Cao, and X. Q. Pan, ACS Appl. Mater. Interfac., **2**, 1060–1065 (2010).
18. H. Hosono, Y. Ogo, H. Yanagi, and T. Kamiya, Electrochem. Solid-State Lett., **14**, H13–H16 (2011).
19. H. Yabuta, N. Kaji, R. Hayashi, *et al*., Appl. Phys. Lett., **97**, 072111 (2010).
20. X. Du, Y. Du, and S. M. George, J. Vacuum Sci. Technol. A: Vacuum, Surfaces, and Films, **23**, 581–588 (2005).
21. A. Huda, C. T. Handoko, M. D. Bustan, *et al*., Mater. Lett., **211**, 293–295 (2018).
22. E. V. Spesivtsev, S. V. Rykhlitskii, and V. A. Shvets, Optoelectron., Instrum. Data Process., **47**, No. 5, 419–425 (2017).
23. Z. R. Dai, J. L. Gole, J. D. Stout, and Z. L. Wang, J. Phys. Chem. B, **106**, 12741279 (2002).
24. Z. Galazka, R. Uecker, D. Klimm, *et al*., Phys. Status Solidi A, **211**, No. 1, 6673 (2014).